Gyrokinetic simulation of turbulence driven geodesic acoustic modes in edge plasmas of HL-2A tokamak

Feng Liu,[1,a)] Z. Lin,[2] J. Q. Dong,[1,3] and K. J. Zhao[1]
[1]*Southwestern Institute of Physics, Chengdu 610041, China*
[2]*Department of Physics and Astronomy, University of California, Irvine, California 92697, USA*
[3]*Institute for Fusion Theory and Simulation, Zhejiang University, Hangzhou 310027, China*

(Received 13 May 2010; accepted 7 September 2010; published online 29 November 2010)

Strong correlation between high frequency microturbulence and low frequency geodesic acoustic mode (GAM) has been observed in the edge plasmas of the HL-2A tokamak, suggesting possible GAM generation via three wave coupling with turbulence, which is in turn modulated by the GAM. In this work, we use the gyrokinetic toroidal code to study the linear and nonlinear development of the drift instabilities, as well as the generation of the GAM (and low frequency zonal flows) and its interaction with the turbulence for realistic parameters in the edge plasmas of the HL-2A tokamak for the first time. The simulation results indicate that the unstable drift wave drives strong turbulence in the edge plasma of HL-2A. In addition, the generation of the GAM and its interaction with the turbulence are all observed in the nonlinear simulation. The simulation results are in reasonable agreement with the experimental observations. © *2010 American Institute of Physics*.
[doi:10.1063/1.3496981]

I. INTRODUCTION

Anomalous cross field particle, momentum, and energy transport in tokamak plasma are generally believed to arise from the microturbulence excited by drift wave instabilities, such as ion/electron temperature gradient driven modes and trapped electron mode (TEM). Identifying the underlying mechanism and searching for the ways to suppress the turbulence is one of the key topics in magnetic fusion studies. One of the major progress made in this field in recent years is the identification of zonal flows (ZFs).[1] ZFs are self-generated large scale coherent structures, resulting from parametric instabilities and regulating the turbulence. It plays a crucial role in setting the level of turbulence and associated transport and has been under intensive investigation in magnetically confined fusion plasmas in the past decades. It is widely accepted that there are two types of zonal flows: one is the low frequency ZF, the other is the higher frequency oscillation called the geodesic acoustic mode (GAM).[2] The experimental identification and characteristics of ZFs and GAMs have recently been reported in a variety of toroidal fusion devices.[3] The structure in poloidal cross section and characteristics of the flows were studied at the edge in the DIII-D tokamak and in the core of the JIPP-TIIU tokamak plasma.[4–7] The radial and poloidal structures of the GAM oscillations were investigated in ASDEX and in T-10 device.[8,9] Recently, the toroidal symmetry (n=0) of the GAM/ZFs has been identified in the edge plasmas of the HL-2A tokamak.[10] Strong correlation between the high frequency microturbulence and the low frequency GAM has also been observed,[11] suggesting the possibility of GAM generation by turbulence and turbulence modulation by GAM.[12] Much experimental research has been done to explore the physics mechanism leading to turbulent transport, ZF generation, and its role in transport reduction in the HL-2A tokamak.[13–16] However, simulation study about ZFs and turbulence of the HL-2A experiments has not been performed.

In this work, we use the gyrokinetic toroidal code (GTC),[1] which has been effectively used for studies of turbulent transport and zonal flow in tokamak plasmas, to simulate the linear and nonlinear development of the drift wave instabilities, such as ion/electron temperature gradient driven modes and TEM, as well as the generation of GAM (and low frequency zonal flows) and its interaction with the turbulence for realistic parameters, including steep pressure gradients and large safety factor q in edge plasmas of the HL-2A tokamak for the first time. In the GTC linear simulation without collision effect, we find that the TEM is strongly unstable in the edge plasma of the HL-2A tokamak. The TEM instability is driven by the electron density and temperature gradients. Meanwhile, the GAM structure and its regulation of the turbulence are found in the nonlinear simulation. The frequency of the GAM from the simulation is about tens of kilohertz, which is close to the experimental observations and theoretical value. The properties of the GAM, such as the radial wavenumber and frequency spectrum, are investigated and compared with the observations of the HL-2A experiments.

The remainder of this paper is organized as follows. The simulation model is described in Sec. II. The simulation results are given in Sec. III. Finally, Sec. IV is devoted to the conclusions.

II. SIMULATION MODEL

In the electrostatic gyrokinetic particle simulations using GTC,[1] the plasma is treated as a set of computational particles interacting with each other through self-generated elec-

a)Electronic mail: liuf@swip.ac.cn.

 © 2010 American Institute of Physics

trostatic fields. The gyrokinetic equations describing toroidal plasmas in GTC are formulated as follows:[17,18]

$$\frac{d}{dt}f_\alpha(\boldsymbol{X},\mu,v_\parallel,t) \equiv \left[\frac{\partial}{\partial t} + \dot{\boldsymbol{X}}\cdot\nabla + \dot{v}_\parallel\frac{\partial}{\partial v_\parallel}\right]f_\alpha = 0, \tag{1}$$

$$\dot{\boldsymbol{X}} = v_\parallel \boldsymbol{b}_0 + \boldsymbol{v}_E + \boldsymbol{v}_g + \boldsymbol{v}_c, \tag{2}$$

$$\dot{v}_\parallel = -\frac{1}{m_\alpha}\frac{\boldsymbol{B}_0^*}{B_0}\cdot(\mu\nabla B_0 + Z_\alpha\nabla\phi), \tag{3}$$

$$\boldsymbol{B}_0^* = \boldsymbol{B}_0 + \frac{v_\parallel}{\Omega_\alpha}\boldsymbol{b}_0\times\nabla B_0. \tag{4}$$

Here, $f_\alpha(\boldsymbol{X},\mu,v,t)$ is the gyrocenter distribution function in terms of the gyrocenter position $\boldsymbol{X}$, μ is the magnetic moment, $v_\parallel$ is the parallel velocity, the index $\alpha=i,e$ stands for the particle species, Z_α and m_α are the particle electric charge and mass, respectively, $\boldsymbol{B}_0$ is the equilibrium magnetic field, and $\boldsymbol{b}_0\equiv\boldsymbol{B}_0/B_0$ is the unit vector. ϕ is the gyrophase-averaged electrostatic potential. The $\boldsymbol{E}\times\boldsymbol{B}$ drift velocity $\boldsymbol{v}_E$, the ∇B drift velocity $\boldsymbol{v}_g$, and the curvature drift velocity $\boldsymbol{v}_c$ are given by

$$\boldsymbol{v}_E = \frac{c\boldsymbol{b}_0\times\nabla\phi}{B_0}, \tag{5}$$

$$\boldsymbol{v}_g = \frac{1}{m_\alpha\Omega_\alpha}\mu\boldsymbol{b}_0\times\nabla B_0, \tag{6}$$

$$\boldsymbol{v}_c = \frac{1}{\Omega_\alpha}v_\parallel^2\nabla\times\boldsymbol{b}_0. \tag{7}$$

The electrostatic potential ϕ in Eq. (3) is described by gyrokinetic Poisson's equation[19]

$$\frac{4\pi Z_i^2 n_i}{T_i}(\phi-\tilde{\phi}) = 4\pi(Z_i n_i - e n_e), \tag{8}$$

with

$$\tilde{\phi}(x) = \frac{1}{2\pi}\int \phi(\boldsymbol{X})f_{0i}(\boldsymbol{X},\mu,v_\parallel)\,\delta(\boldsymbol{X}-x+\boldsymbol{\rho}_i)d\boldsymbol{X}d\mu dv_\parallel d\sigma, \tag{9}$$

where $n_\alpha=\int f_\alpha d\boldsymbol{v}$ is the gyrophase-averaged gyrocenter density, $\tilde{\phi}$ is the gyroaveraged potential, $f_{0j}(\boldsymbol{X},\mu,v_\parallel)$ is the ion equilibrium gyrocenter distribution function, $\boldsymbol{\rho_i}\equiv-\boldsymbol{v}_{i\perp}\times\boldsymbol{b}_0/\Omega_i$ is the ion gyroradius vector, Ω_i is the ion cyclotron frequency, and σ is the gyrophase angle.

GTC simulation uses the particle-in-cell method to solve the gyrocenter distribution functions and ϕ interactively in the toroidal geometry. For ions, field quantities on the guiding center are averaged over a gyro-orbit. For electrons, the GTC code employs the drift kinetic equation because of the small electron gyroradius. An electrostatic version of the fluid-kinetic electron model is used to overcome numerical difficulty associated with the small electron mass.[20,21] As for the boundary conditions for the field solve, the electrostatic potential is set to zero since we make sure that all the turbulence-driving gradients go smoothly to zero at the boundaries.

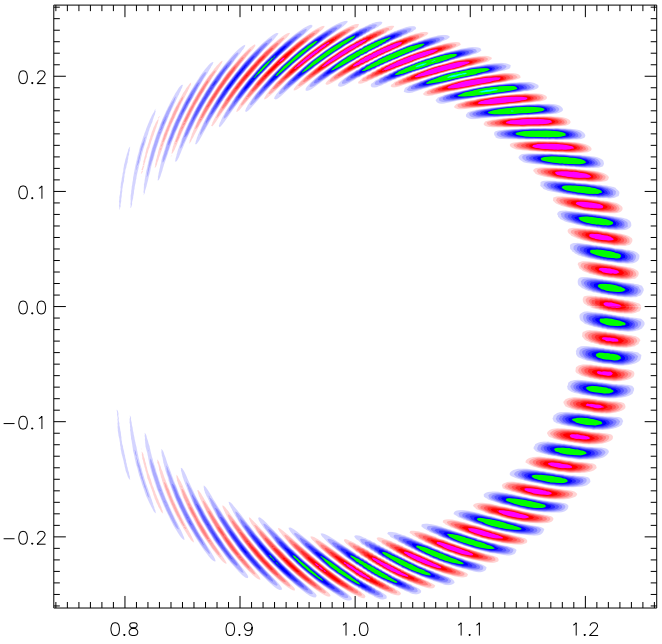

FIG. 1. (Color online) Structure of the electrostatic potential ϕ of the TEM instability in a poloidal cross section.

III. SIMULATION RESULTS

In our GTC simulations, the following HL-2A experiment parameters are used: the major radius $R=1.65$ m, the minor radius $a=0.4$ m, the toroidal magnetic field $B_t=1.4$ T, the plasma current is 180 kA, the densities of ions and electrons at the edge of HL-2A are $n_i=n_e=2.5\times10^{18}$ m^{-3}, and the simulation domain r is limited in the region from $0.84a$ to $1.0a$. $R/L_T=36.2$, $T_i=T_e$, and $R/L_n=39.6$ with the L_T and L_n being the temperature and density gradient scale lengths, respectively, the ion to electron mass ratio is $m_i/m_e=1837$. At the probe location $r=0.92a$ in the experiment, the safety factor is $q=3.6$ and the magnetic shear is assumed to be $s=r/q(dq/dr)=1.0$. The q-profile $q(r)=0.7+2.4r/a+0.83(r/a)^2$ is used in the simulation. In addition, flux surfaces of concentric circular cross sections and uniform marked particles are employed in the current simulation.

A. Linear simulation

Since the linear simulation results in the gyro-Bohm normalized units do not depend on temperature, we start the linear simulation with high temperature of $T_i=T_e=1$ keV. The trapped electron modes are found to be strongly unstable for the above parameters in the edge plasma of HL-2A. No instability is found when electron is assumed to be adiabatic. Shown in Fig. 1 is a contour plot of the electrostatic potential of the TEM instability in a poloidal cross section. The unstable mode structure is weakly ballooning and peaks at the low field side of the torus. The numerically converged growth rate γ and real frequency ω_r versus $k_\theta\rho_i$ is shown in

TABLE I. Mode growth rate γ and real frequency ω_r normalized to v_i/R, ω_*, respectively, for the two cases of $R/L_T=18$, $R/L_n=20$ and $R/L_T=36.2$, $R/L_n=39.6$ when $k_\theta\rho_i=0.3$, 0.6, and 0.9.

$k_\theta\rho_i$	$\gamma\left(\frac{v_i}{R}\right)$	$\gamma(\omega_*)$	$\omega_r\left(\frac{v_i}{R}\right)$	$\omega_r(\omega_*)$
	Case 1: $\frac{R}{L_T}=18$ and $\frac{R}{L_n}=20$			
0.3	2.50	0.417	1.2	0.222
0.6	4.13	0.382	1.06	0.098
0.9	4.70	0.235	−0.71	−0.044
	Case 2: $\frac{R}{L_T}=36.2$ and $\frac{R}{L_n}=39.6$			
0.3	3.36	0.309	3.51	0.323
0.6	6.22	0.286	1.17	0.054
0.9	6.98	0.214	−1.17	−0.036

Table I for the two sets of temperature and density gradients to cover the uncertainty of profile measurements. Here, the frequency of a mode propagating in electron diamagnetic direction is defined as positive, k_θ is the poloidal wavenumber, the growth rate and real frequency are normalized to v_i/R and ω_*, respectively. Here, $v_i=\sqrt{T_i/m_i}$ is the ion thermal speed, $\omega_*=k_\theta\rho_i v_i/L_n$ is the plasma diamagnetic drift frequency. It is clear that the growth rate with low R/L_T and R/L_n is lower than that with high R/L_T and R/L_n. The growth rate and frequency increase and decrease with the increase of $k_\theta\rho_i$, respectively, as is shown in Fig. 2. It indicates that the instability simulated here is driven by the electron temperature and density gradients. Meanwhile, as shown in Table I, the frequency of the TEM in range from $2v_i/R$ to $7v_i/R$ is smaller than the estimated bounce frequency of the trapped electrons $\omega_{be}\simeq\sqrt{a/R}(v_e/qR)=1.1\times10^6/\mathrm{s}$, here v_e is the electron thermal speed. The frequency of the TEM is also much lower than ω_*, which is consistent with the theoretical results.[22] The mode has a fluid characteristic since the growth rate is larger than the real frequency.

B. Nonlinear simulation

In HL-2A experiments, the electron temperature T_e is measured to be in the range from 20 to 70 eV. In our nonlinear simulation, $T_i=T_e=60$ eV is used, in addition to $R/L_T=18$ and $R/L_n=20$.

The time-radial two-dimensional (2D) electric field $E(r,t)$ structure of m=n=0 mode (n and m are the toroidal and poloidal mode numbers, respectively), defining GAM, is shown in Fig. 3(a). The oscillation of GAM is very clear, and the GAM mode propagates both inward and outward in the radial direction but dominated by the outward propagation. The fact that GAM dominates over the low frequency ZF is consistent with the lower GAM damping rate in the high-q region, while in the low-q region ZF dominates since the GAM is strongly damped.[23,24] This can be seen from the simplified formula of the GAM damping rate,[24]

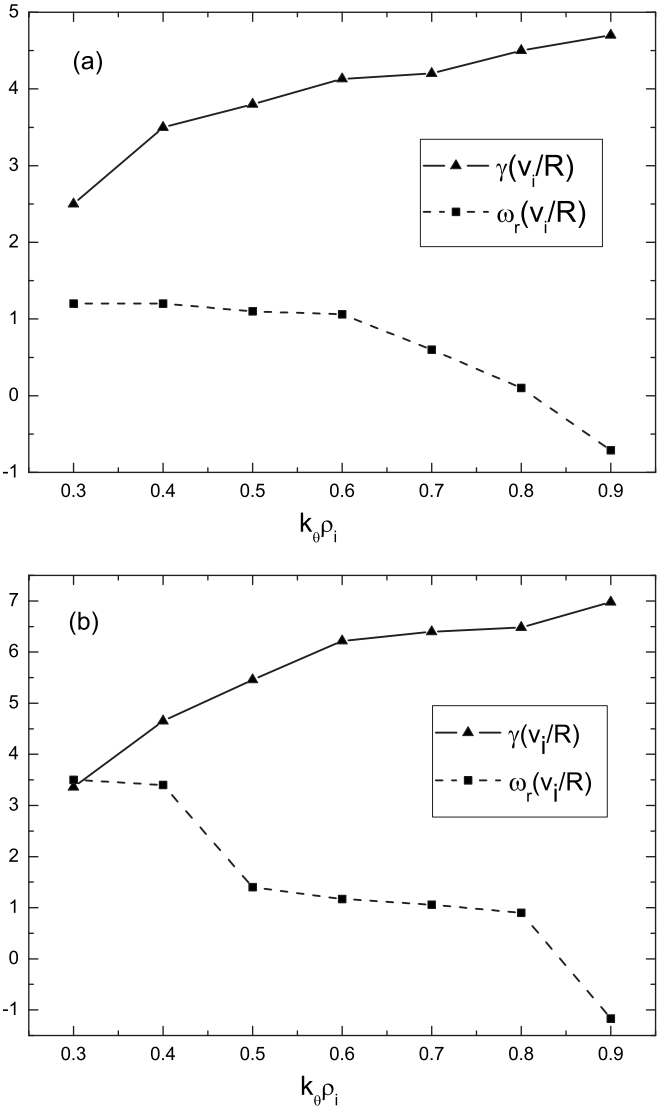

FIG. 2. Mode growth rate γ and real frequency ω_r vs $k_\theta\rho_i$ for (a) $R/L_T=18$, $R/L_n=20$ and (b) $R/L_T=36.2$, $R/L_n=39.6$.

$$\gamma_{\mathrm{GAM}}=\frac{\pi^{1/2}}{2}\frac{v_i}{R}\frac{(R\omega_{\mathrm{GAM}}/v_i)^6}{7/4+\tau}q^5\exp\left[-\left(\frac{qR\omega_{\mathrm{GAM}}}{v_i}\right)^2\right]. \tag{10}$$

Here, $\tau=T_e/T_i$, the frequency of GAM ω_{GAM} is given by[24]

$$\omega_{\mathrm{GAM}}^2=\left(\frac{7}{4}+\tau\right)\frac{v_i^2}{R^2}\left[1+\frac{46+32\tau+8\tau^2}{(7+4\tau)^2q^2}\right]. \tag{11}$$

At a fixed radial location in Fig. 3(a), the frequency of GAM is calculated roughly as about $1.9v_i/R\sim14$ kHz, which is comparable with the experimental observation of tens of kilohertz, and close to the theoretical value of $1.66v_i/R$ from Eq. (11).

The evolutions of the flux surface averaged turbulence potential intensity and the electric field of GAM at the flux surface of $r=0.92a$ are given in Fig. 3(b). It is clearly shown that at the beginning, the turbulence grows first and then drives the GAM which develops with a time delay. Later on, the turbulence decays while the GAM electric field grows

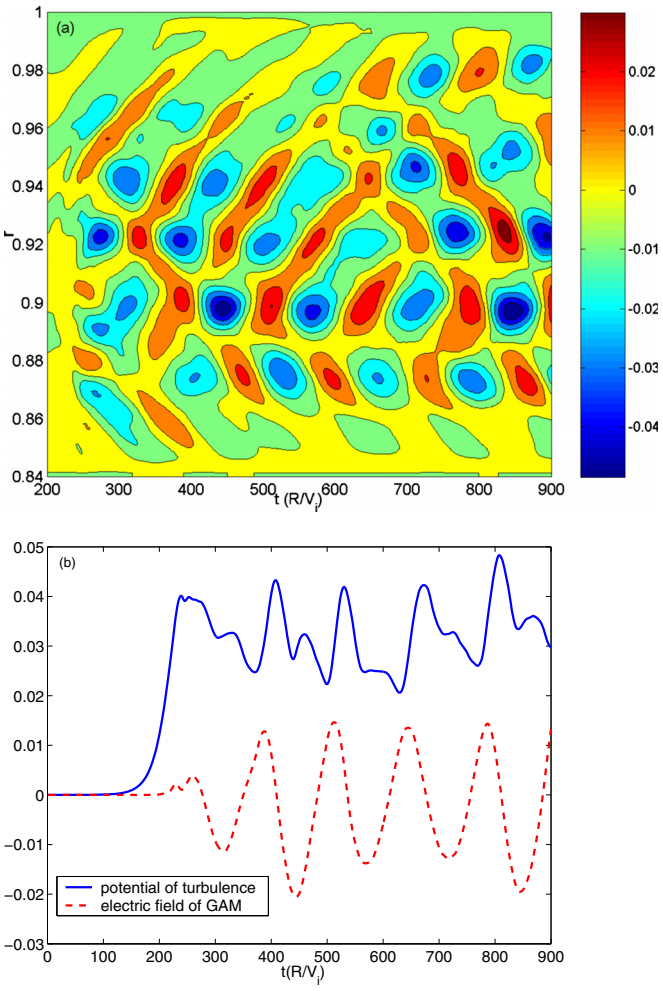

FIG. 3. (Color online) The electric field E_r structure of the GAM in the time-radial plane (a) and the time evolutions of the flux surface averaged turbulence intensity (blue solid line) and zonal flow electric field on one flux surface (red dotted line) (b).

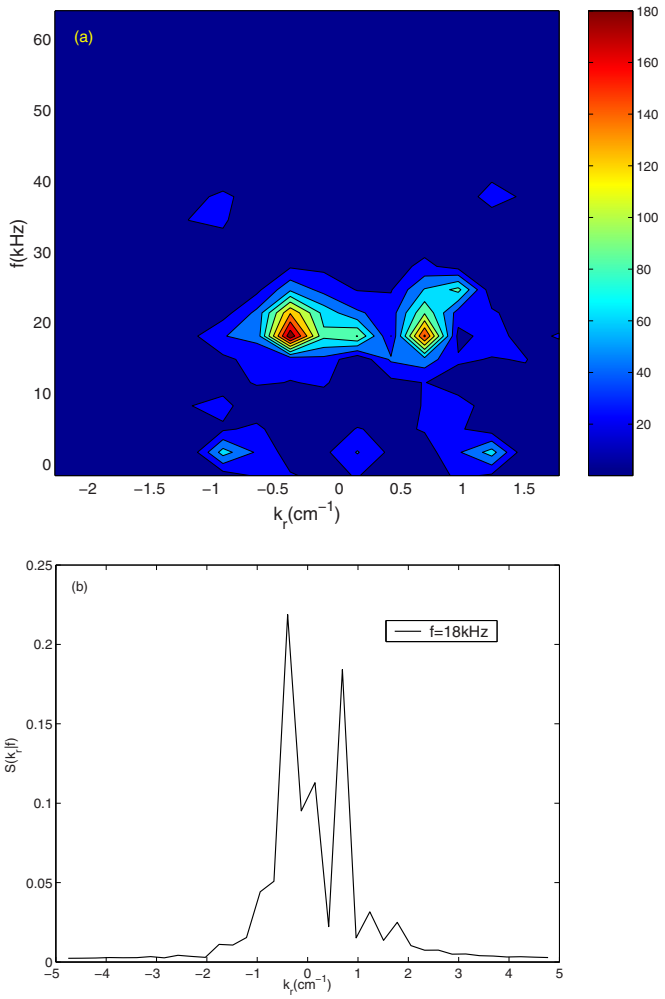

FIG. 4. (Color online) The radial wavenumber-frequency spectrum $S(k_r,f)$ (a) and the radial wave vector spectrum $S(k_r|f)$ at $f=18$ kHz (b) of the GAM electric field.

up, and the turbulence grows again while the GAM decays. This indicates strongly that the turbulence is modulated by the GAM electric field and demonstrates a prey-predator relationship between the turbulence and GAM. Presumably, both negative and positive peaks of GAM should have equal effects on the turbulence. However, it seems that here they do not. Nevertheless, the simulation results do indicate that the turbulence decreases when a negative peak of GAM grows. The unresolved question is that a negative peak does not correspond to a dip of turbulence as a positive peak does. One possible reason is that the turbulence energy here is averaged over the whole simulation volume, while the GAM electric field is on a single flux surface. This should be explored more in detail in the future.

The spectral structures of the GAM can be characterized with the wavenumber-frequency spectrum $S(k_r,f)$ which is defined as

$$S(k_r,f) = \left| \int \int S(r,t) e^{-i\omega t} e^{-ik_r r} dt dr \right| .$$

Here, $S(r,t)$ is either the electric field or potential of GAM in time-radial 2D plane. The contour plot of the spectrum $S(k_r,f)$ for GAM electric field $E(r,t)$ as given in Fig. 4(a) shows that the E_r flows are almost symmetric with respect to the k_r axis. Meanwhile, the peak of the spectrum is at about 0.7 cm^{-1} in the positive k_r direction and at about 18 kHz in the frequency domain.

We can also see it from Fig. 4(b), which gives the radial wave vector spectrum $S(k_r|f)$ of GAM electric field $E(r,t)$ at $f=18$ kHz, where $S(k_r|f)=S(k_r,f)/S(f)$ and $S(f)=\Sigma_{k_r} S(k_r,f)$. There are two peaks in the $S(k_r|f)$ spectrum, and the peak in the positive k_r region is located at about 0.7 cm^{-1}. These results are very close to the observation of experiments.[16]

The contour plot of the spectra $S(k_r,f)$ and $S(k_r|f)$ for GAM potential $\phi_{00}(r,t)$ are given in Figs. 5(a) and 5(b), respectively. From Fig. 5(a), we can see that the peak of the spectrum $S(k_r,f)$ is also located at about 18 kHz, the same as spectrum $S(k_r,f)$ of the electric field. The radial wave vector spectrum of GAM frequency is almost symmetric with both positive and negative components, but the former is slightly larger than the latter. Although the spectrum $S(k_r,f)$ of electric field and potential of GAM are different in the vicinity of $k_r=0$ because $E_r=-ik_r\phi$, both of them indicate that GAM propagates more outward in the radial direction. The simula-

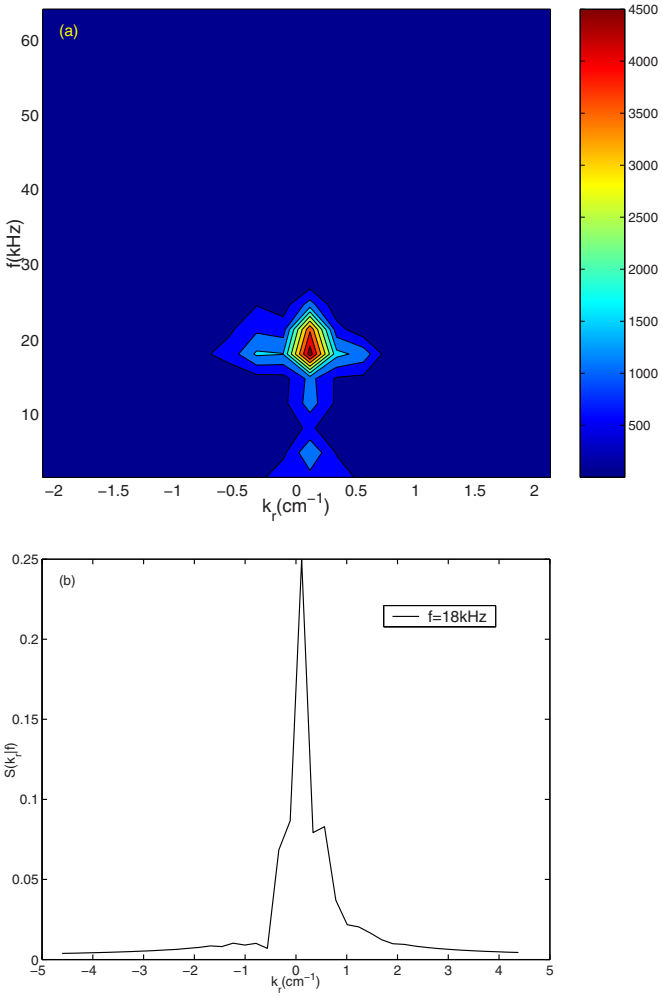

FIG. 5. (Color online) The radial wavenumber-frequency spectrum $S(k_r,f)$ (a) and the radial wave vector spectrum $S(k_r|f)$ at $f=18$ kHz (b) of the GAM potential.

tion results do not exactly reproduce the experimental observations but have some similarity. A clear similarity is that the peak in the negative k_r region is lower and closer to the $k_r=0$ point than the peak in the positive k_r region. This indicates that the GAM packet predominantly propagates outward. The wavenumber width of the GAM flow estimated from the spectrum $S(k_r|f)$ is $\Delta k_r=1.5$ cm^{-1}, as shown in Fig. 5(b). The agreement between the simulation results and the experimental observations is quite reasonable considering that the data used in the simulation are not exactly the same as in Ref. 16.

IV. CONCLUSIONS

In this paper, we carry out the global gyrokinetic toroidal code GTC simulation with the real parameters of HL-2A experiment for the first time. The linear results show that there is an unstable TEM in the edge plasmas of HL-2A experiments, and the unstable mode is driven by the electron temperature and density gradients. Meanwhile, the frequency of TEM is much lower than the electron diamagnetic drift frequency, which is in agreement with the theoretical results. In the nonlinear simulations, we find that GAM structures exist in the edge plasmas of HL-2A tokamak. The frequency of the GAM is about tens of kilohertz, the radial wave vector k_r is about 0.7 cm^{-1}. Both are comparable with the observations in the experiments. In addition, the evolutions of the turbulence intensity and GAM electric field show clearly the evidence that the GAM/ZF has modulation effects on the turbulence. The results also show that the GAM propagates both inward and outward in radial direction, but dominated by the outward propagation. Furthermore, the GAM is found to dominate over the low frequency ZF and regulate the edge turbulence in HL-2A with a large safety factor q.

ACKNOWLEDGMENTS

This work is supported by the U.S. Department of Energy (DOE), SciDAC GSEP, and GPS Centers, the National Basic Research Program of China under Grant No. 2008CB717806, and the ITER Project in China under Grant No. 2009GB105005.

We acknowledge the useful discussions with W. L. Zhang, Y. Xiao, and H. S. Zhang.

[1] Z. Lin, T. S. Hahm, W. W. Lee, W. M. Tang, and R. B. White, Science **281**, 1835 (1998).
[2] N. Winsor, J. L. Johnson, and J. M. Dawson, Phys. Fluids **11**, 2448 (1968).
[3] A. Fujisawa, T. Ido, A. Shimizu, S. Okamura, K. Matsuoka, H. Iguchi, Y. Hamada, H. Nakano, S. Ohshima, K. Itoh, K. Hoshino, K. Shinohara, Y. Miura, Y. Nagashima, S.-I. Itoh, M. Shats, H. Xia, J. Q. Dong, L. W. Yan, K. J. Zhao, G. D. Conway, U. Stroth, A. V. Melnikov, L. G. Eliseev, S. E. Lysenko, S. V. Perfilov, C. Hidalgo, G. R. Tynan, C. Holland, P. H. Diamond, G. R. McKee, R. J. Fonck, D. K. Gupta, and P. M. Schoch, Nucl. Fusion **47**, S718 (2007).
[4] M. Jakubowski, R. J. Fonck, and G. R. McKee, Phys. Rev. Lett. **89**, 265003 (2002).
[5] G. R. McKee, R. J. Fonck, M. Jakubowski, K. H. Burrell, K. Hallatschek R. A. Moyer, W. Nevins, D. L. Rudakov, and X. Xu, Plasma Phys. Controlled Fusion **45**, A477 (2003).
[6] G. R. McKee, D. K. Gupta, R. J. Fonck, D. J. Schlossberg, M. W. Shafer, and P. Gohil, Plasma Phys. Controlled Fusion **48**, S123 (2006).
[7] Y. Hamada, A. Nishizawa, T. Ido, T. Watari, M. Kojima, Y. Kawasumi, K. Narihara, K. Toi, and JIPPT-IIU Group, Nucl. Fusion **45**, 81 (2005).
[8] G. D. Conway, B. Scott, J. Schirmer, M. Reich, A. Kendl, and the ASDEX Upgrade Team, Plasma Phys. Controlled Fusion **47**, 1165 (2005).
[9] V. A. Vershkov, D. A. Shelukhin, S. V. Soldatov, A. O. Urazbaev, S. A. Grashin, L. G. Eliseev, A. V. Melnikov, and the T-10 Team, Nucl. Fusion **45**, S203 (2005).
[10] Y. Liu, X. T. Ding, Q. W. Yang, L. W. Yan, D. Q. Liu, W. M. Xuan, L. Y. Chen, X. M. Song, Z. Cao, J. H. Zhang, W. C. Mao, C. P. Zhou, X. D. Li, S. J. Wang, J. C. Yan, M. N. Bu, Y. H. Chen, C. H. Cui, Z. Y. Cui, Z. C. Deng, W. Y. Hong, H. T. Hu, Y. Huang, Z. H. Kang, B. Li, W. Li, F. Z. Li, G. S. Li, H. J. Li, Q. Li, Y. G. Li, Z. J. Li, Yi Liu, Z. T. Liu, C. W. Luo, X. H. Mao, Y. D. Pan, J. Rao, K. Shao, X. Y. Song, M. Wang, M. X. Wang, Q. M. Wang, Z. G. Xiao, Y. F. Xie, L. H. Yao, L. Y. Yao, Y. J. Zheng, G. W. Zhong, Y. Zhou, and C. H. Pan, Nucl. Fusion **45**, S239 (2005).
[11] K. J. Zhao, T. Lan, J. Q. Dong, L. W. Yan, W. Y. Hong, C. X. Yu, A. D. Liu, J. Qian, J. Cheng, D. L. Yu, Q. W. Yang, X. T. Ding, Y. Liu, and C. H. Pan, Phys. Rev. Lett. **96**, 255004 (2006).
[12] K. Hallatschek and D. Biskamp, Phys. Rev. Lett. **86**, 1223 (2001).
[13] K. J. Zhao, J. Q. Dong, L. W. Yan, W. Y. Hong, T. Lan, A. D. Liu, J. Qian, J. Cheng, D. L. Yu, Y. Huang, H. D. He, Yi Liu, Q. W. Yang, X. R. Duan, X. M. Song, X. T. Ding, and Y. Liu, Phys. Plasmas **14**, 122301 (2007).
[14] K. J. Zhao, J. Q. Dong, L. W. Yan, W. Y. Hong, Q. Li, J. Qian, J. Cheng, A. D. Liu, H. L. Zhao, D. F. Kong, Yi Liu, Y. Huang, X. M. Song, X. T. Ding, Q. W. Yang, X. R. Duan, and Y. Liu, Nucl. Fusion **49**, 085027 (2009).
[15] T. Lan, A. D. Liu, C. X. Yu, L. W. Yan, W. Y. Hong, K. J. Zhao, J. Q.

Dong, J. Qian, J. Cheng, D. L. Yu, and Q. W. Yang, Phys. Plasmas **15**, 056105 (2008).
[16]A. D. Liu, T. Lan, C. X. Yu, H. L. Zhao, L. W. Yan, W. Y. Hong, J. Q. Dong, K. J. Zhao, J. Qian, J. Cheng, X. R. Duan, and Y. Liu, Phys. Rev. Lett. **103**, 095002 (2009).
[17]T. S. Hahm, Phys. Fluids **31**, 2670 (1988).
[18]I. Holod, W. L. Zhang, Y. Xiao, and Z. Lin, Phys. Plasmas **16**, 122307 (2009).
[19]W. Lee, J. Comput. Phys. **72**, 243 (1987).
[20]Z. Lin, Y. Nishimura, Y. Xiao, I. Holod, W. L. Zhang, and L. Chen, Plasma Phys. Controlled Fusion **49**, B163 (2007).
[21]Z. Lin and L. Chen, Phys. Plasmas **8**, 1447 (2001).
[22]J. Q. Dong, S. M. Mahajan, and W. Horton, Phys. Plasmas **4**, 755 (1997).
[23]Y. Xiao and Z. Lin, Phys. Rev. Lett. **103**, 085004 (2009).
[24]Z. Gao, K. Itoh, H. Sanuki, and J. Q. Dong, Phys. Plasmas **15**, 072511 (2008).